Astroparticle Physics 109 (2019) 12–24

Contents lists available at ScienceDirect

Astroparticle Physics

journal homepage: www.elsevier.com/locate/astropartphys

Atmospheric monitoring and inter-calibration of the telescope optical throughput efficiencies using the trigger rates of the Cherenkov Telescope Array

Stanislav Stefanik[a,*], Dalibor Nosek[a], Raquel de los Reyes[b,c], Markus Gaug[d], Petr Travnicek[e]

[a] Institute of Particle and Nuclear Physics, Faculty of Mathematics and Physics, Charles University, V Holesovickach 2, 180 00 Prague 8, Czech Republic
[b] Max Planck Institut für Kernphysik, Saupfercheckweg, Heidelberg, Germany
[c] German Aerospace Center, Earth Observation Center, Wessling, D-82234, Germany
[d] Unitat de Física de les Radiacions, Departament de Física, and CERES-IEEC, Universitat Autónoma de Barcelona, Bellaterra, E-08193, Spain
[e] Institute of Physics of the Czech Academy of Sciences, Na Slovance 1999/2, 182 21 Prague, Czech Republic

ARTICLE INFO

Article history:
Received 6 August 2018
Revised 1 February 2019
Accepted 7 February 2019
Available online 10 February 2019

Keywords:
Air showers
Atmospheric monitoring
Calibration
Cherenkov telescopes
Gamma-ray astronomy

ABSTRACT

We discuss a calibration method for imaging atmospheric Cherenkov telescope arrays, based on the detection of cosmic rays. The focus lies on the monitoring of transmission of Cherenkov light in the atmosphere and on the relative calibration of telescope optical throughput efficiencies. We present an approach that addresses both issues by surveying and comparing trigger rates of telescopes in a stereoscopic configuration. A Monte Carlo feasibility study was conducted to explore dependencies of stereo trigger rates on the array layout and observing conditions of the Cherenkov Telescope Array (CTA). Analytical expressions for most of these dependencies have been found and implemented in an extension of the method of the Cherenkov Transparency Coefficient (CTC). In the investigated examples, the resolution of the method for the atmospheric and array calibration has been shown to be 4% and 4–7%, respectively.

1. Introduction

Indirect detection of very-high-energetic (VHE; ≥ 0.02 TeV) cosmic rays (CRs) and γ-rays is based on their interaction with the air molecules in the Earth's atmosphere. CRs induce air showers of relativistic particles which can be sampled by ground-based detectors. Specifically, imaging atmospheric Cherenkov telescopes (IACTs) are designed to catch Cherenkov light that is emitted when charged particles in the air showers pass through the atmosphere. The focus of the IACTs lies on the detection of γ-rays which can be correlated with their source of origin and allow to study extreme astrophysical environments.

The energy of primary particles is deduced from intensities of recorded shower images which are compared with Monte Carlo (MC) simulations for reference observation conditions. Shower images at a given energy are subject to variations due to changing atmospheric and hardware conditions. Various atmospheric phenomena can cause attenuation of Cherenkov light leading to a reduced number of photons at the detector level. Similarly, degradation of optical and photodetection elements of a telescope results in decreased detection efficiency of the instrument. Either of these effects, or both simultaneously, can result in an underestimation of the primary particles' energies, and in the mis-reconstruction of the energy spectrum of astrophysical sources. These implications are not unavoidable systematic effects and can be mitigated by robust schemes aimed at the monitoring of the atmospheric extinction and the optical properties of telescopes.

The Cherenkov Telescope Array[1] (CTA) is the next generation IACT facility currently under construction [1]. In the VHE γ-ray regime, CTA will aim at unprecedented flux sensitivity, angular and energy resolution through the deployment of tens of telescopes of different sizes in two locations in the Northern (CTA-N) and Southern (CTA-S) hemispheres. Three principal classes of telescopes are expected to be part of the system to cover a wide γ-ray energy window. Currently, there are several different designs of the optical system and hardware of telescopes. Medium-size telescopes (MSTs) with mirror dish diameters of the order of 12 m will cover the energy range between ~ 0.08 and 50 TeV. The detection of low energy γ-rays (≥ 0.02 TeV) will be mediated by a few large-size telescopes (LSTs) with a diameter of the order of 23 m. An extensive array of small-size telescopes (SSTs) with diameters of about

* Corresponding author.
E-mail address: stefanik@ipnp.troja.mff.cuni.cz (S. Stefanik).

[1] http://www.cta-observatory.org.

https://doi.org/10.1016/j.astropartphys.2019.02.002
0927-6505/

4 m, foreseen only for the CTA-S site, is designed to cover the high energy regime of the spectrum (1–300 TeV).

In order to achieve its scientific objectives, CTA has established requirements on the maximum systematic uncertainties on the reconstructed energy of an individual γ-ray event and the global energy scale which should be less than 15% and 10% [2], respectively. To meet these requirements, CTA has established a calibration strategy which encompasses several instruments and methods for the atmospheric monitoring as well as the assessment of the telescope optical throughput [2–4]. The approaches for atmospheric calibration make use of the Lidars [5] in combination with the stellar photometry [6]. Furthermore, All-Sky-Cameras [7] and Sun/Moon photometry [8] are used to characterize the atmospheric conditions.

Optical throughput calibration in CTA includes methods using direct observational data both at the individual telescope level, based on the analysis of muon ring images [9,10] and reconstructed parameters of air showers [11,12], and at the array level using the reconstructed electron spectrum [13]. In addition to these methods, optical throughput calibration can be performed utilizing instruments with calibrated light sources illuminating the telescopes either from a portable ground-based device [14] or an airborne calibration platform [15]. Furthermore, a possibility of calibrating the CTA telescopes with vertically propagating laser pulses has been investigated [16].

In this paper, we present a complementary method included uniquely in both strategies on atmospheric and array calibration in CTA. Our approach utilizes the number of air showers registered per unit time by a telescope system (trigger rate). Trigger rates of Cherenkov telescopes are dominated by the detection of charged cosmic ray particles, in particular primary protons which constitute the bulk of cosmic rays detected in the GeV–TeV energy range.

The method builds upon the concept of the Cherenkov Transparency Coefficient (CTC) developed within the phase I of the H.E.S.S. experiment [17] which employed four telescopes of identical design. The CTC was introduced as a monitoring quantity to estimate the transparency of the atmosphere to Cherenkov light using data taken by IACTs during scientific observations. The method does not require any additional equipment or special calibration data acquisition which would interfere with regular data taking. The accuracy of the CTC in H.E.S.S. was shown to be 9% for the cloudless time periods.

The CTC needs, however, further development in order to be applied to complex telescope arrays with more stringent requirements on the measurement precision, as will be the case of CTA. Telescope multiplicity, geometrical layout and pointing directions have to be accounted for in order to keep the CTC independent of array realization and observation conditions. The number of all possible combinations of telescopes producing a stereo trigger is going to increase significantly in CTA compared to current systems. Taking into account every combination of sub-arrays of active telescopes and pointing directions would constitute a computationally challenging task to find a suitable set of scaling factors for each observation mode, if one would follow the H.E.S.S. approach. Instead, we investigate here an update of the CTC algorithm which preserves its simplicity and universality without the need for large sets of look-up parameters.

In addition to the usage of the CTC for atmospheric monitoring, we examine here the possibility of employing this concept for the relative calibration of telescope optical throughput efficiencies. An extensive air shower observed simultaneously by different telescopes should generate an identical response in all telescopes at the same distance to the shower if their detection efficiencies are correctly accounted for. Calibration of the optical throughput of telescopes of a same type in the whole array (intercalibration) can be achieved through the comparison of outcomes of telescope measurements if camera detection efficiencies have been properly calibrated. Provided a locally stratified atmosphere, i.e. the attenuation of photons is uniform across the array, the atmospheric transparency to Cherenkov light can be considered a calibration quantity identical for all telescopes, similarly to other inter-calibration approaches using shower parameters [11,12]. Utilizing this assumption without the knowledge of the precise value of the atmospheric transparency, we demonstrate a method of calibration of the relative optical efficiencies. This approach can serve as a cross-check for other array calibration methods.

The structure of the paper is as follows. In Section 2, we explain a new method for the CTC calculation in large telescope arrays. In Section 3, the application of the CTC for the purposes of atmospheric and array calibration is discussed. Using a production of dedicated MC simulations of air showers summarized in Section 3.3, we discuss various phenomena that affect the trigger rates of Cherenkov telescopes, and thus the CTC estimates, in Section 4. In Section 5, we test the performance of the calibration method using simulations of the candidate array layout for the CTA-N site. A discussion of the obtained results is given in Section 6. The paper is concluded in Section 7.

2. A new definition of the Cherenkov transparency coefficient

2.1. Background

The CTC is designed as a measure of the atmospheric transparency (T) to Cherenkov light given by the ground layer aerosol optical depth[2] (τ), i.e. $T \propto \exp(-\tau)$. The concept of the CTC utilizes the dependency of the telescope trigger rate on the atmospheric extinction of photons while eliminating other effects due to the observation and hardware conditions (discussed in Section 4). The CTC is defined in H.E.S.S. phase I as [17]

$$\hat{T} = \frac{1}{N \cdot k_N} \sum_{i=1}^{N} \frac{R_i^{\frac{1}{1.7}}}{\mu_i \cdot g_i}, \tag{1}$$

where R_i is the trigger rate of the ith telescope, μ_i describes the telescope photon detection efficiency determined from the analysis of muon ring images [4] and g_i is the average pixel gain of the telescope. The sum runs over N telescopes participating in the observation, $i = 1, 2 \ldots N$, and k_N is the multiplicity correction accounting for different detection rates depending on N.

To ensure independence from instrumental effects, the trigger rates are corrected for the state of the telescope hardware. The reflectivity of the optical elements (e.g. mirrors, light cones) and the efficiency of the camera sensors determine the optical throughput efficiency of a telescope. The product of the photon detection efficiency (μ_i) with the average camera pixel gain (g_i) is invariant with respect to gain mis-calculation and sensitive only to the optical properties of the telescope.

Variations of the single telescope trigger rate are also caused by random fluctuations due to the accidental triggers or the night sky background (NSB). In order to suppress these fluctuations, only events that trigger at least two telescopes in coincidence (stereoscopic detection) are read out by the acquisition system. In the H.E.S.S. approach, the stereo trigger rate of each telescope (R_i in Eq. (1)) is determined from all events recorded by it together with any other active telescope in the array. The CTC is calculated in observation runs[3] in which either three or four telescopes are active,

[2] The aerosol optical depth (τ) at a wavelength λ is defined as the aerosol extinction coefficient (α) integrated over the height of a vertical air column, $\tau(\lambda) = \int_h^H \alpha(\lambda, z)\mathrm{d}z$, where H is the light emission altitude and h is the observer's altitude.

[3] Observation run refers to a single time period of continuous data taking in current IACT systems, typically $\sim$20–30 min.

depending on the trigger configuration. The stereo trigger rates are then normalized using a set of look-up values (k_N in Eq. (1), where $N = 3, 4$) in order to account for the differences between the total numbers of telescopes in individual runs.

Unless the array layout is a regular polygon and all telescope detection efficiencies are equivalent, some instruments can trigger in stereo mode more often than others. This can happen either because of the larger number of telescopes in their proximity or due to the better photon detection efficiency of their closest neighbors. In complex arrays, where telescopes may be split into sub-arrays that independently observe different targets, the number of possible combinations of active telescopes is significantly higher. Following the H.E.S.S. approach, unique layout-dependent factors would have to be calculated for each observation configuration in order to account for the difference between the stereo trigger rates. In the CTA case, it is not feasible to use the stereo trigger rates ascertained from all events recorded by a particular telescope regardless of the other instrument in coincidence.

Instead, we assume the trigger rates of events detected by chosen pairs of telescopes, R_{ij}, where $i \neq j$. For each observation, different pairs are identified by the set of active telescopes of the same type. An air shower event is assigned to, possibly more than one, telescope pair only if it was recorded by both considered instruments. The stereo trigger rate for every chosen pair is given by the total number of events associated with it divided by the duration of observation. In addition to accounting for the detection efficiency of one telescope as in Eq. (1), we assume that the hardware state of the second telescope in the pair also affects the stereo trigger rate.

2.2. Estimation

The minimum energy of the primary CR particle detectable by IACTs (trigger energy threshold, E_{th}) is inversely proportional to the atmospheric transparency, $E_{\mathrm{th}} \propto T^{-1}$, in the first order when neglecting altitude dependencies of the atmospheric absorber. The rate of registered events is approximately determined by the differential CR flux ($J(E)$) weighted by the effective trigger area ($A_{\mathrm{eff}}(E)$) of the instrument, i.e. $R \propto \int_{E_{\mathrm{th}}}^{\infty} J(E) A_{\mathrm{eff}}(E) \mathrm{d}E$. Hence, the integral trigger rate depends on the atmospheric transparency as $R \propto E_{\mathrm{th}}^{-\gamma} \propto T^{\gamma}$, where γ derives from the spectral index of the differential energy spectrum of CR particles. In the following, we adopt the value of $\gamma = 1.7$ corresponding to the flux of CR protons ($J(E) \propto (E/\mathrm{TeV})^{-2.7}\ \mathrm{m^{-2}\,s^{-1}\,TeV^{-1}\ sr^{-1}}$ [18]).

In order to stabilize the trigger rates, we consider the rates recorded by a pair of telescopes of the same type (R_{ij}, where i, j assign different telescopes). For a given telescope pointing direction,[4] the trigger rate is roughly constant provided that the detection efficiency does not change considerably within the observation run. A trigger rate estimate, $\hat{R}_{ij}(\mathcal{O}, \varepsilon_i, \varepsilon_j)$, can be obtained assuming that the rate dependencies on the observation conditions, $\mathcal{O}$ (e.g. the geometrical configuration, the Earth's magnetic field, see Section 4), and on the telescope detection efficiencies, ε_i, $\varepsilon_j \in [0, 1]$, are well reproduced from MC simulations. Considering a linear dependence of the pairwise stereo trigger rate on the detection efficiencies of both involved telescopes (for details see Section 4.4), the trigger rate estimate can be expressed as $\hat{R}_{ij}(\mathcal{O}, \varepsilon_i, \varepsilon_j) = \varepsilon_i \cdot \varepsilon_j \cdot \hat{R}^0_{ij}(\mathcal{O})$, where $\hat{R}^0_{ij}$ is the estimate obtained from MC simulations assuming non-degraded telescope efficiencies ($\varepsilon_i = \varepsilon_j = 1$).

[4] We note that variations of the stereo trigger rate can be caused by a non-negligible change in the zenith angle when tracking a particular object in the sky during a typical observation run of ~20–30 min in duration.

In the following, ε_i refers to part of the nominal telescope optical throughput, assuming that the average pixel gain is properly calibrated and fixed when estimating the optical throughput with inherent gain dependency.

Variations of the experimental trigger rate (R_{ij}) with respect to its estimate ($\hat{R}^0_{ij}$) combined with the detection efficiencies (ε_i, ε_j) are representative of changes in the true atmospheric transparency to Cherenkov light, T. A pairwise estimate of the atmospheric transparency is given by

$$\hat{T}_{ij}(\tau) = \frac{1}{\mathcal{K}} \left(\frac{R_{ij}(\tau, \mathcal{O}, \varepsilon_i, \varepsilon_j)}{\varepsilon_i \cdot \varepsilon_j \cdot \hat{R}^0_{ij}(\mathcal{O})} \right)^{\frac{1}{\gamma}}, \tag{2}$$

where i and j are the unique identifiers of telescopes of the same type, τ is the aerosol optical depth and $\mathcal{K}$ is the normalization for the reference atmospheric conditions.

Using the trigger rates registered for many different telescope pairs, a set of aerosol transparency estimates ($\hat{T}_{ij}$) is obtained. The Cherenkov Transparency Coefficient is then given as an average of these pairwise estimates, i.e.

$$\hat{T} = \frac{1}{P} \sum_{\substack{i=1 \\ i<j}}^{N} \hat{T}_{ij} = \frac{1}{P \cdot \mathcal{K}} \sum_{\substack{i=1 \\ i<j}}^{N} \left(\frac{R_{ij}}{\varepsilon_i \cdot \varepsilon_j \cdot \hat{R}^0_{ij}} \right)^{\frac{1}{\gamma}}, \tag{3}$$

where the sum runs over all P pairs in the array of N active telescopes.

The trigger rate estimates ($\hat{R}^0_{ij}$, see Appendix A) together with one normalization factor ($\mathcal{K}$) constitute a set of a few look-up values which allow for the generalization of the CTC concept to a wide range of observation conditions. This is in contrast to finding a large set of unique scaling factors for each configuration as utilized in the H.E.S.S. approach (k_N in Eq. (1)).

In Eqs. (2)–(3) and throughout the paper, we adopted the following notation. Let ν denote a true value of a variable (e.g. atmospheric transparency, intrinsic detector efficiency, etc.). A hat symbol, $\hat{\nu}$, denotes the estimate of a true value of a variable ν derived according to our method. Specifically, $\hat{\nu}^0$ refers to the estimate of the value on the assumption of a telescope in a nominal state (i.e. no change in the detection efficiency has occurred). Since no CTA experimental data are yet available, we simulated MC data for which this notation applies as well.

3. Applications of the CTC

3.1. Atmospheric monitoring

Various atmospheric phenomena affect propagation of Cherenkov light in the air and, thus, observations by IACTs. The atmospheric attenuation of light happens through extinction of photons by aerosols, clouds and molecules. Furthermore, the molecular density profile affects the development of the air showers and the emission of Cherenkov light [19,20]. To characterize the contribution of these effects on the energy reconstruction and effective area, several instruments and methods have been devised within the atmospheric calibration strategy in CTA [3,21].

Relying on direct observational data of telescopes, the concept of the CTC can be used in CTA alongside other approaches. The CTC estimates ($\hat{T}$) calculated according to Eq. (3) allow to monitor changes in the aerosol optical depth, or equivalently, the atmospheric transparency (T) to photons around the energy threshold. A necessary prerequisite for the CTC calculation is the knowledge of the telescope optical efficiencies ε_i. These have to be estimated by independent means of absolute calibration, e.g. through the analysis of Cherenkov light registered from local muons [4,9,10].

Provided that the telescope responses have been correctly accounted for, the CTC is independent of instrumental and observational effects. Its evolution is then indicative of changes in the atmospheric transparency to Cherenkov light due to variations in the aerosol concentrations and clouds.

3.2. Inter-calibration of telescope responses

A reliable calibration of the telescope optical throughput efficiencies is necessary for the reconstruction of air shower events. In contrast with other methods [4], relative inter-calibration of the telescope efficiencies can be performed utilizing the optical throughput dependency of the pairwise estimates of the atmospheric transparency ($\hat{T}_{ij}$ in Eq. (2)).

The estimates $\hat{T}_{ij}$ are sensitive to variations of the optical throughput efficiency, given by fractions ε_i, ε_j of the nominal values for telescopes assigned as i, j. Pairwise estimates of the atmospheric transparency in Eq. (2) can be expressed as

$$\hat{T}_{ij} = \frac{\hat{T}^0_{ij}}{\left(\varepsilon_i \cdot \varepsilon_j\right)^{\frac{1}{\gamma}}}, \tag{4}$$

where $\hat{T}^0_{ij}$ is the transparency estimate obtained for nominal telescope efficiencies ($\varepsilon_i = \varepsilon_j = 1$). We are concerned with the case when the individual optical efficiencies are not known. Provided that the atmospheric conditions are uniform across the array of telescopes observing in a same direction, the pairwise transparency estimates $\hat{T}_{ij}$ are assumed to equal the same value of the true atmospheric transparency T for all telescope pairs, $\hat{T}_{ij} = T; \forall i, j$. Treating efficiencies ε_i as free parameters, the inter-calibration of responses of telescopes of the same type can be achieved by minimisation of the objective function (similarly as in [12]):

$$F(\varepsilon, T) = \sum_{\substack{i=1 \\ i<j}}^{N} \frac{\left(\hat{T}^0_{ij} - \left(\varepsilon_i \cdot \varepsilon_j\right)^{\frac{1}{\gamma}} \cdot T\right)^2}{\sigma^2_{ij}}, \tag{5}$$

where σ_{ij} are the uncertainties of the known pairwise estimates $\hat{T}^0_{ij}$ and the sum runs over all selected pairs in the sub-array of N telescopes.

As a result of the minimisation, a set of reconstructed optical efficiencies, $\hat{\varepsilon}_i$, is obtained. It should be emphasized that the inter-calibration is performed in a relative manner since the actual value of the atmospheric transparency is not known a priori. The transparency T is considered a free parameter and there is an ambiguity in the absolute values of $\hat{\varepsilon}_i$. The efficiency of one telescope is arbitrarily chosen as a reference and not varied throughout the minimisation routine. No other assumptions about the remaining optical efficiencies and the atmospheric transparency are necessary as long as the number of telescope pairs chosen for the inter-calibration is equal to or greater than the number of active telescopes. The relative calibration does not depend on the exact value of the reference efficiency (ε_R). However, the absolute values of recovered estimates of $\hat{\varepsilon}_i$ and $\hat{T}$ are functions of ε_R. The reference efficiency should be chosen as a result of an independent measurement (e.g. [14,15]) if absolute estimates of optical throughput are to be obtained.

The outlined inter-calibration method does not attempt to estimate the optical throughput of telescopes and the atmospheric transparency at the same time. The calculation of the CTC requires the knowledge of the absolute telescope optical efficiencies, which need to be estimated by other array calibration methods and input in Eq. (3). The inter-calibration utilizing the equivalence of the CTC for all telescopes is then considered a backup procedure applied independently of the atmospheric monitoring strategy (Section 3.1). This approach may be of particular interest for a quick verification of other estimates of optical efficiencies.

3.3. Monte Carlo simulations

We use MC simulated data as experimental CTA data are not yet available. For the study of the stereo trigger rate dependencies, we carried out MC simulations of air showers initiated by protons. Telescope specifications were defined as in the CTA simulation production [22]. CORSIKA [23] and *sim_telarray* software [24] were used for the simulations of air showers and telescopes, respectively. Used geometrical definitions are summarized in Fig. 1.

The study is focused on the CTA-N site for which only two telescope types, the LSTs and MSTs, are foreseen. Telescopes were simulated in various configurations that were optimized for the investigation of individual dependencies, but they are not considered candidate layouts for CTA-N. The full CTA-N layout (Fig. 2), consisting of 4 LSTs and 15 MSTs, was simulated for the purpose of a test of our method in Section 5.

The camera trigger in our simulations is based on the sum trigger logic [25,26]. Signals within a group of adjacent camera pixels are added together and compared with the given threshold value. In our configuration, the MST (LST) cameras were divided into overlapping patches of 9 (21) pixels each. The camera was read out if the summed signal of any of these patches was above a predefined threshold. A minimum of two telescopes was required to trigger within a coincidence time window in order to issue a system level trigger.

The energy spectrum of primary protons was simulated in the energy range 0.004–100 TeV with a spectral index of −2.0. For each studied scenario, 5×10^8 air showers were simulated and then divided into bins of true energy and distance of the shower axis to the centroid of the telescope pair (impact parameter). Pairwise trigger efficiencies were calculated binwise using subsets of events readout by the system which triggered predefined pairs of telescopes. The number of such events divided by the number of MC air showers in the bin gives the pairwise trigger efficiency. This efficiency weighted by the energy spectrum of CRs [18] and integrated over the energy and the impact parameter yields the trigger rate of the considered telescopes.

The Earth's magnetic field was fixed to a small value ($\mathcal{O}(10^{-3}\ \mu T)$) in the simulations summarized in Sections 4.1 and 4.2 in order to study only the geometrical dependencies of the stereo trigger rates. Effects of the magnetic field were then included in all subsequent calculations by setting the field intensity to the value corresponding to the CTA-N location. The optical efficiency of telescopes was fixed to its nominal value ($\varepsilon = 1$) in all particular studies except for Section 4.4 where the dependence of the trigger rate on telescope hardware is investigated. Numbers of simulated air showers were the same in all scenarios, i.e. with and without the magnetic field as well as for different telescope optical efficiencies.

The atmospheric transmission of light in the wavelength range 200–1000 nm was set using the tables created by the MODTRAN program [27]. The tables contain values of the optical depth τ as a function of the incident light wavelength λ for a range of emission altitudes. Corresponding approximately to the CTA-N site, we assumed an observation altitude of 2150 m above sea level. All results in Section 4 were obtained for the same reference atmospheric model assuming tropical atmosphere and navy maritime extinction of light. Various models of the optical depth, providing various atmospheric transparencies, were assumed only for the test of the CTC method in Section 5. A single air density profile

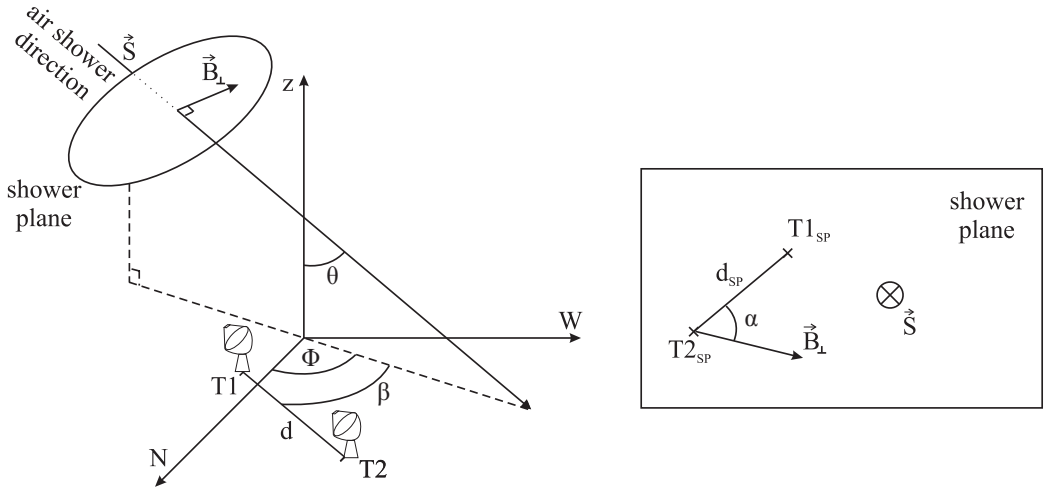

Fig. 1. Definitions used in this study. The zenith angle (θ) of the air shower is measured between the momentum vector of the incident CR particle and the vertical axis. The azimuth angle (ϕ) is defined between the magnetic North and the horizontal projection of the shower direction. The angle β is defined between the horizontal projection of the shower direction and the line joining a pair of telescopes (T1, T2), separated by a distance d. Orthogonal to the shower direction ($\vec{S}$) is the shower plane. Projections from the ground plane into the shower plane are indexed with SP. The angle α is defined between the component of the magnetic field perpendicular to the shower direction ($\vec{B}_\perp$) and the shower-plane projection of the line joining the telescopes.

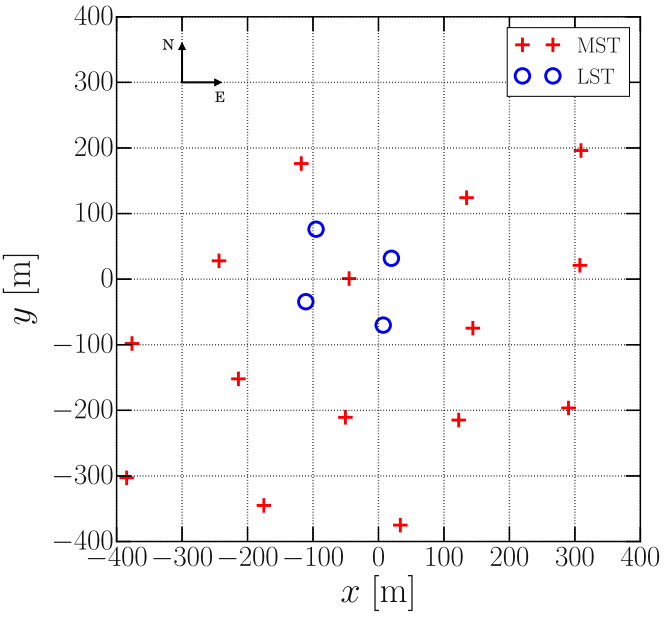

Fig. 2. CTA-N array layout simulated in this study. Positions of the 4 LSTs (blue circles) and 15 MSTs (red crosses) are shown in the horizontal plane. The telescope mounts were simulated at different altitudes in the range 2157–2230 m given by the topography of the CTA-N site.

was used for all simulations since its variations are expected to have a negligible effect on the trigger rates compared to the atmospheric phenomena we intend to calculate and monitor with the CTC.

It is worth noting that the CTC is an integral measure of the optical depth up to the production height of the CR-initiated air showers. It accounts for the whole interval of wavelengths accessible by IACTs. For a meaningful comparison of the recovered CTC values with the initially assumed atmospheric transparency, we adopt the following convention. Assuming that the influence of atmospheric absorbers on IACTs is mostly significant below the maximum of Cherenkov emission from air showers, we consider the reference optical depth ($\tau(\lambda)$) corresponding to the altitude of 12 km.[5] The atmospheric transparency assumed in MC simulations is stated as the median value of the product of $\exp(-\tau(\lambda))$ with the wavelength-dependent nominal mirror reflectivity and the efficiency of the camera sensors.[6] The resulting values for individual atmospheric models are normalized so that $T = 1.0$ corresponds to the case without any attenuation due to aerosols.

4. Stereo trigger rate

We study trigger rate dependencies $R(\mathcal{O})$ on observation conditions $\mathcal{O}$. Specifically, we deal with the zenith angle (θ), the inter-telescope distance (d), the alignment of the shower direction with respect to the telescope pair (β) and the geomagnetic field ($\vec{B}$), see Fig. 1. Furthermore, the dependence of the stereo trigger rate on the state of the telescope hardware (ε) is explored. All following findings relate to the estimate of the trigger rate $\hat{R}(\mathcal{O}, \varepsilon)$.

The results comprise examples from the MC study which were derived for the MSTs. A concurrent study was performed also for the LSTs, yielding similar results which are not discussed here.

4.1. Zenith angle

We consider the relationship between the zenith angle of observations (θ) and the stereo trigger rates of IACTs. The area on the ground illuminated by Cherenkov light from the air showers increases as $\propto (\cos\theta)^{-2}$. This affects the stereo trigger rates in two ways:

- The trigger rate decreases with growing zenith angle due to the decrease in the ground density of Cherenkov photons which are spread across a larger area. This is demonstrated in the top panel in Fig. 3 in the case of a small separation of telescopes ($d = 160$ m) where one can notice that the trigger rate starts to decrease at $\theta \sim 40°$.

[5] The maximum of Cherenkov radiation occurs below ~12 km for air showers initiated by vertically impacting photons with energy $E \geq 10$ GeV [19] (note that the maximum is lower for CRs).

[6] Photomultiplier tubes are foreseen for the cameras of the LSTs and the MSTs of the Davies–Cotton design. Silicon photomultipliers are envisaged for the SSTs and the MSTs of the Schwarzschild–Couder design.

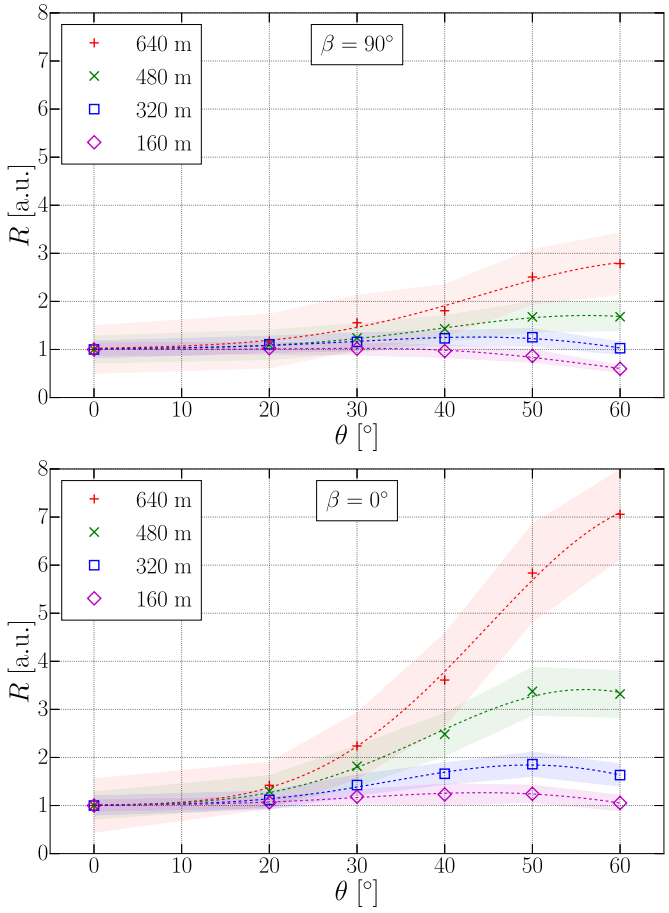

Fig. 3. Stereo trigger rate as a function of the zenith angle θ of proton-initiated air showers with a fixed azimuth angle $\phi = 0°$. The line joining a pair of telescopes was either parallel ($\beta = 0°$, bottom panel) or orthogonal ($\beta = 90°$, top panel) to the shower direction. Colors and markers denote different separations of telescopes and contours indicate the statistical uncertainties of trigger rates. Dashed lines represent the results of the fit described in Appendix A. (For interpretation of the references to color in this figure legend, the reader is referred to the web version of this article.)

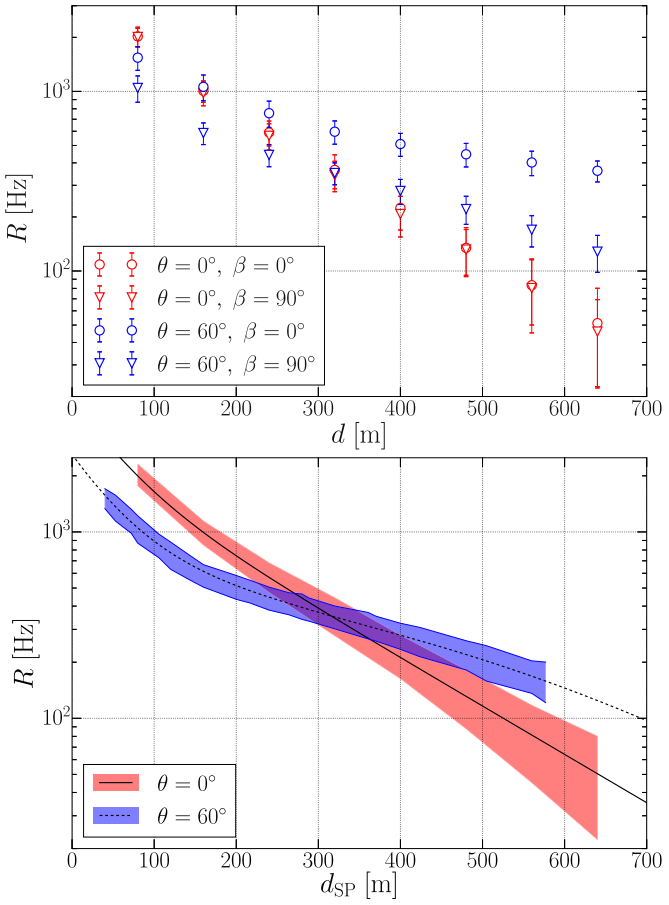

Fig. 4. Stereo trigger rate as a function of telescope pair separation in the horizontal plane, d (top), and separation in the shower plane, d_{SP} (bottom). Colors differentiate between zenith angles $\theta = 0°$ (red) and 60° (blue). Markers denote different alignments of telescope pairs represented by the angle β between the shower horizontal direction and the line joining the telescopes. Contours in the bottom panel indicate the statistical uncertainties of the rates from the top panel. (For interpretation of the references to color in this figure legend, the reader is referred to the web version of this article.)

- The effective area for the stereoscopic detection of air showers increases with the zenith angle. This is of small importance for telescopes separated up to about 200 m. The trigger rate of more distant detectors can be several times higher at large zenith angles compared to $\theta = 0°$, see Fig. 3.

The trigger rate in Fig. 3 is normalized to $R(\theta = 0°) = 1$ in order to compare its dependence on the zenith angle for different inter-telescope distances. The dashed lines in Fig. 3 depict the results of fits to the data which are elaborated in Appendix A.

4.2. Telescope alignment and separation

With regard to the observations under different zenith angles, we examine the dependence of the stereo trigger rates on the direction of an air shower in the horizontal plane. Related to this, we consider also the influence of the inter-telescope distance.

The section of the Cherenkov light cone with the ground plane can be roughly approximated either by a circle ($\theta = 0°$) or by an ellipse with varying eccentricity ($\theta > 0°$). For $\theta > 0°$, the trigger probability for two telescopes in coincidence depends on the angle between the major axis of the ellipse illuminated by Cherenkov light and the line joining the telescopes. In Fig. 3, the trigger rate is shown for orthogonal (top panel) and parallel (bottom panel) alignment of telescope pairs with respect to the air shower direction (angle β in Fig. 1). Differences between various alignments are more pronounced for large separations of telescopes, compare the red data points ($d = 640$ m) for $\theta > 30°$ in both panels in Fig. 3, for example.

Fig. 4 demonstrates the influence of the telescope alignment on the stereo trigger rate considered as a function of the inter-telescope distance for $\theta = 0°$ and 60° (see also [28]). In the case of vertical incidence ($\theta = 0°$, red data points), no significant difference in trigger rates is observed between parallel ($\beta = 0°$, circles) and perpendicular ($\beta = 90°$, triangles) orientations of the telescope pair with respect to the air shower direction. At $\theta = 60°$ (blue markers), the variation of the trigger rate with the alignment of telescopes depends on their inter-distance. In the studied range of telescope separations ($d \in [0\,\text{m}, 640\,\text{m}]$), the trigger rate in the parallel configuration is roughly $1.5 - 3$ times greater than in the orthogonal case, see the top panel in Fig. 4.

The conic section of the Cherenkov radiation is roughly circular in the plane perpendicular to the air shower direction. The symmetry of the trigger rate with the telescope alignment is restored when the inter-telescope distance, instead of in the ground plane (d), is expressed in terms of a projection in the shower plane (d_{SP} in Fig. 1). This projection is equivalent to the separation of the telescope pointing directions and is given as

$$d_{SP}(\theta, \beta) = d \cdot \sqrt{1 - \sin^2\theta \cdot \cos^2\beta}. \quad (6)$$

Utilizing Eq. (6), the data from the top panel in Fig. 4 can be re-stated in terms of d_{SP}, shown in the bottom panel of Fig. 4. The dependence of the stereo trigger rate on the zenith angle can be parametrized for any alignment angle of telescopes by a single equation, see Appendix A. An estimate of the trigger rate is then obtained ($\hat{R}^0(\theta, d_{SP})$, shown by the lines in the bottom panel in Fig. 4) for any possible geometrical configuration (d, θ, β). Such estimates are valid if the influence of the geomagnetic field can be neglected.

4.3. Earth's magnetic field

The development of the air cascades initiated by CRs as well as the distribution of emitted Cherenkov light is affected by the Earth's magnetic field [29–32]. Here, we focus on the variations of stereo trigger rates due to the geomagnetic field.

Charged particles in the air showers are deflected due to the action of the Lorentz force governed by the component of the magnetic field perpendicular to their momentum vectors ($\vec{B}_\perp$). Assuming that the majority of particles move roughly along the direction of the shower axis, the perpendicular component is parallel with the shower plane (see Fig. 1) and is a function of the observation direction, $\vec{B}_\perp = \vec{B}_\perp(\phi, \theta)$. In Fig. 5, the size of the perpendicular component ($B_\perp$) at the CTA-N site relative to the total magnitude of the geomagnetic field (B_N) is shown as a function of (ϕ, θ).

Particles of opposite charges are deflected in the opposite directions orthogonal to $\vec{B}_\perp$ and their momentum vectors. The lateral extent of Cherenkov photons on the ground increases with $\vec{B}_\perp$ for air showers developing under a given zenith angle. This results in the overall decrease of the photon density on the ground. However, the Cherenkov light yield may locally increase further away from the shower axis in the directions perpendicular to $\vec{B}_\perp$ compared to the case $|\vec{B}| = B \simeq 0$.

Considering the estimates $\hat{R}^0(\theta, d_{SP})$ (see Appendix A) as an approximation of the trigger rate for $B \simeq 0$, we inspect the uncertainties in these estimates caused by the influence of the Earth's magnetic field. The geomagnetic field in the MC simulations was set correspondingly to the CTA-N site[7] as $\vec{B_N} = [30.5, -3.0, 23.8]$ μT. Variations of the trigger rates were investigated for zenith angles $\theta \in \{10°, 37°, 53°\}$ chosen approximately equidistantly in $\cos\theta$. In each case, azimuth angles were chosen such that the resulting configurations cover uniformly the possible outcomes of the perpendicular component $B_\perp$. The number of studied configurations increases with the zenith angle as the range of possible equally spaced values of $B_\perp$ is the largest around $\theta = 55°$, see Fig. 5. In Fig. 6, the ratio $R/\hat{R}^0(\theta, d_{SP})$ is shown as a function of d_{SP}, where R is the MC trigger rate in the realistic case $B = B_N$.

The statistical uncertainties of the individual estimates are depicted by solid error bars in Fig. 6. These maximum uncertainties are shown for the separation $d_{SP} = 400$ m and range from 15% to 20%, depending on the value of θ. The uncertainties at $d_{SP} = 50$ m are typically of the order of $10 - 15$%. The inaccuracies correspond to the numbers of simulated events in several bins of energy and impact parameter. We investigated the reduction of uncertainties in the eventuality of obtaining a 100 times larger set of events. To this end, numbers of simulated showers in each bin were multiplied by a random number from a Poisson distribution with the expected value of 100. The resultant uncertainties of the ratios $R/\hat{R}^0$ are then within about 2% as demonstrated by the dashed error bars in Fig. 6.

Considering the trend of $R/\hat{R}^0$, the average values taken over all inter-telescope distances in Fig. 6 indicate a decrease of the trigger rate with increasing $B_\perp$. We also infer that the variations of the trigger rate with respect to the estimated value ($\hat{R}^0$) depend on the angle α (see Fig. 1) between $\vec{B}_\perp$ and the projection of the line joining the telescopes into the shower plane, as can be seen by comparing the left and right panels in Fig. 6. The particles in the air shower are deflected perpendicular to $\vec{B}_\perp$. If the line joining the telescopes is also perpendicular to $\vec{B}_\perp$ ($\alpha = 90°$), there is a higher Cherenkov light yield and, therefore, higher stereo trigger rate for more distant telescopes than in the case of a parallel alignment ($\alpha = 0°$).

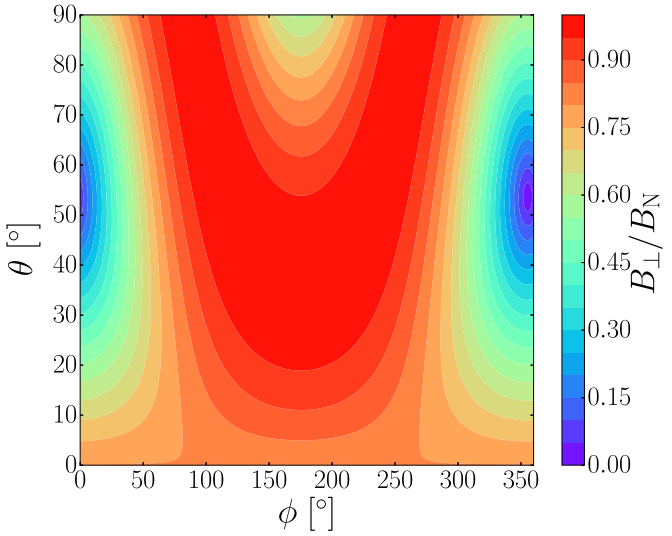

Fig. 5. Fraction of the total size of the Earth's magnetic field vector at the CTA-N location (B_N) corresponding to the component ($B_\perp$) perpendicular to the air shower direction given by the azimuth (ϕ) and zenith (θ) angles.

As it is difficult to approximate the contribution of the geomagnetic field for all different configurations, we refrain from adopting another effective correction for the effects of the field. The data in Fig. 6 provide an estimate of the systematic uncertainties introduced when the magnetic field is neglected. A restriction on the specific configurations of observations can be imposed in order to keep the uncertainties on $\hat{R}^0$ below a given limit. For example, only observations with (ϕ, θ, d_{SP}) satisfying $B_\perp/B_N < 0.5$ can be chosen for the calibration using the CTC so that the variations of $R/\hat{R}^0$ are within $\sim$5%, see e.g. the panels for $\theta = 37°$ and 53° in Fig. 6.

Finally, it is worth noting that the total size of the geomagnetic field vector at the CTA-S site (B_S) is smaller than that of the CTA-N location, i.e. $B_S \approx 0.6 B_N$. Thus, there are more CTA-S than CTA-N configurations (ϕ, θ, d_{SP}) for which $B_\perp$ is smaller than a given value.

4.4. Hardware

Having eliminated the influence of the observation conditions ($\mathcal{O}$), we are concerned now with the hardware dependence of the stereo trigger rates. The state of the telescope hardware, comprising the optical and photo-detection elements, determines the efficiency of the Cherenkov photon detection ε. Here, we inspect the hardware dependence by varying the optical efficiencies of telescopes from their nominal values while keeping the gain of camera sensors fixed in the simulations.

The trigger energy threshold (E_{th}, see Section 2.2) is assumed to be determined by the telescope recording the least Cherenkov light. The amount of detected light is a combined effect of the telescope detection efficiency and the number of Cherenkov photons from the air shower impacting the telescope. The latter changes event-wise and is, in the first order approach for air showers of the

[7] https://www.ngdc.noaa.gov/geomag-web/#igrfwmm (2017).

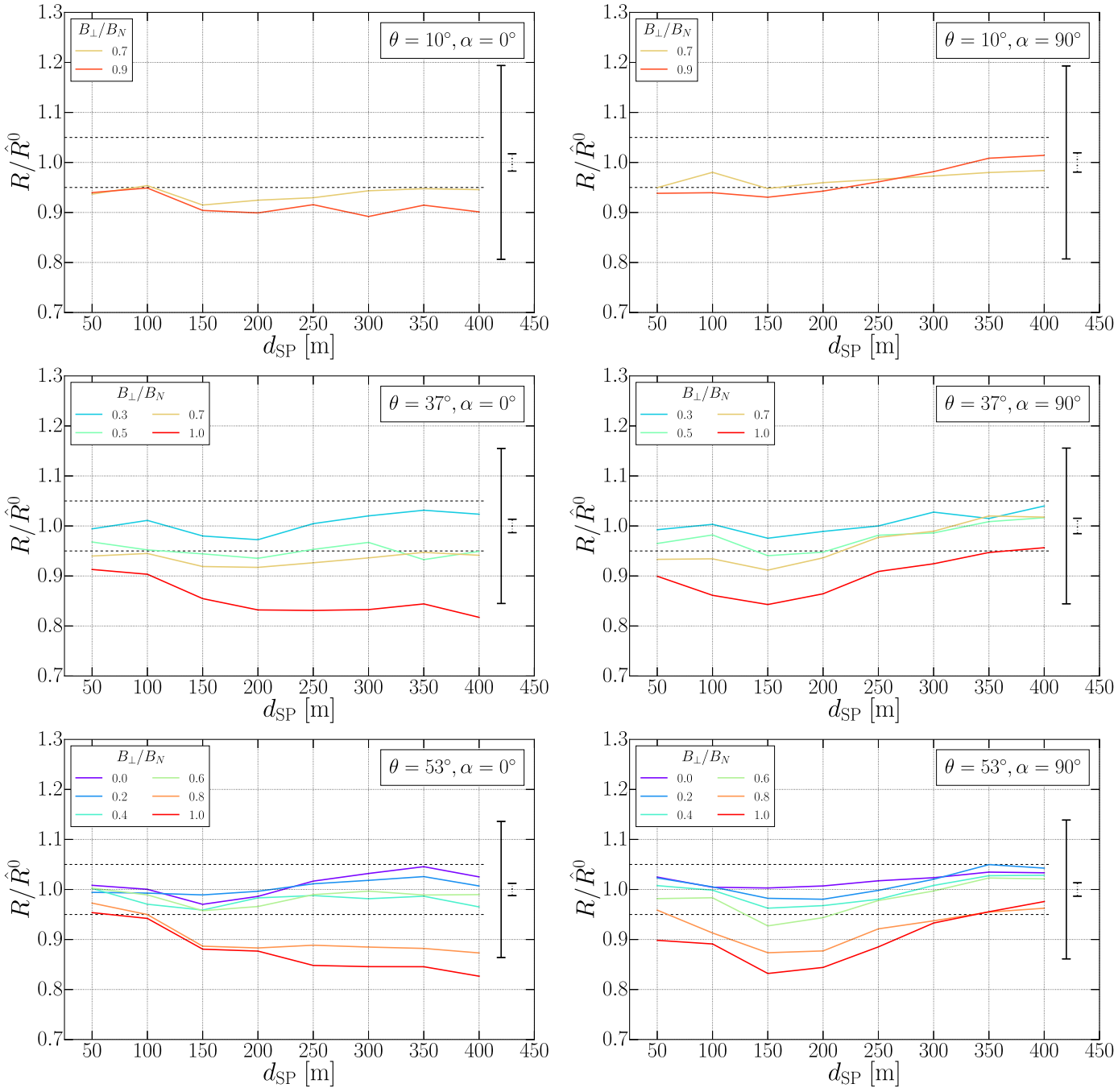

Fig. 6. Ratio $R/\hat{R}^0$ as a function of the inter-telescope distance in the shower plane (d_{SP}). $\hat{R}^0(\theta, d_{SP})$ are the fitted values given by Eqs. (A.1)–(A.5) for $B \simeq 0$. Colors divide the data according to the relative size of the geomagnetic field component perpendicular to the air shower direction ($B_\perp/B_N$). The distributions are shown for three different zenith angles (rows) and two orientations of telescope pair relative to $\vec{B}_\perp$ (columns). The range of configurations shown in each panel is given by the range of possible values of $B_\perp/B_N$ for a given zenith angle (see Fig. 5). Dashed lines depict 5% difference of $\hat{R}^0$ compared to R. Error bars on the right sides of plots illustrate the maximum statistical uncertainties of data (solid) and the change of these uncertainties when the number of simulated events increases approximately hundred times (dashed). (For interpretation of the references to color in this figure legend, the reader is referred to the web version of this article.)

same energy, given by the position of the telescope with respect to the shower core. Motivated by these arguments, we explore the dependence of the trigger rate of two telescopes in coincidence on the optical throughput efficiencies of both. Additionally, the number of photons arriving at a telescope is affected by their attenuation in the atmosphere. We consider the atmospheric extinction to be uniform for the same pointing directions of telescopes, and thus decreasing the number of photons by a same factor for both telescopes in the given pair.

In Fig. 7, the trigger rate of two telescopes is shown as a function of the product of their respective optical efficiencies $\varepsilon_1 \cdot \varepsilon_2$ for a fixed observing zenith angle (here $\theta = 20°$). Efficiencies selected from the interval [0.3, 1.0] refer to the simulated degradation of telescope optical components relative to the specifications ($\varepsilon = 1$). In all instances, the telescope positions were fixed at $d_{SP} = 150$ m.

The trigger rate of a telescope pair appears to be proportional to the product $\varepsilon_1 \cdot \varepsilon_2$. This behavior stems from the complex superposition of all instances when either of the two telescopes deter-

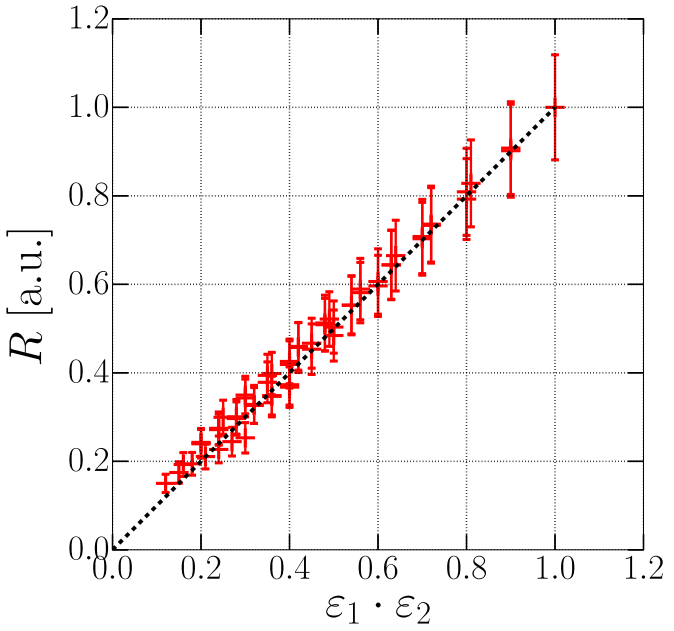

Fig. 7. The trigger rate of two telescopes in coincidence at a distance $d_{SP} = 150$ m as a function of the product of the telescope-wise mirror degraded efficiencies. Proton showers incident at the zenith angle $\theta = 20^\circ$ are used. All rates were normalized by a value of the maximum trigger rate in the simulated data set. The dashed line represents the equality $R = \varepsilon_1 \cdot \varepsilon_2$.

mines the trigger threshold of the pair. In order to account for this dependence, we adopt the linear approximation $\hat{R}_{ij}(\theta, d_{SP}, \varepsilon_i, \varepsilon_j) \approx \varepsilon_i \cdot \varepsilon_j \cdot \hat{R}^0_{ij}(\theta, d_{SP})$ as an effective description of the stereo trigger rate.

5. Test of the CTC method

We tested our new approach to the CTC concept, described in Section 2, utilizing simulations of the full CTA-N array (see Fig. 2). The chosen observation configurations were $B_\perp/B_N = 0.3$ and 0.5 (0.01 and 0.5) for the azimuth angles $\phi = 3^\circ$ and 319° (355° and 33°), respectively, for the zenith angles $\theta = 37^\circ$ (53°). The air shower directions with $B_\perp/B_N \leq 0.5$ were selected, in order to restrict the systematic uncertainty due to the action of the geomagnetic field. The zenith angles were chosen as in Section 4.3, excluding the angle of 10° for which $B_\perp/B_N > 0.5$ in all azimuth directions. For a given zenith angle, the azimuth angle was chosen such that $B_\perp/B_N$ equals either 0.5 or the lowest possible value. In order to have a different optical efficiency for each telescope, degraded optical efficiencies were drawn from the normal distribution $\mathcal{N}(0.7, 0.1)$.

As a first step, we perform the relative inter-calibration of the optical throughput efficiencies in Section 5.1. Then, using the set of reconstructed efficiencies, the CTC is calculated as a measure of the atmospheric transparency, see Section 5.2.

5.1. CTC as an inter-calibration method

The results inferred for the stereo trigger rates in Section 4 were used to obtain the trigger rate estimates, $\hat{R}^0(\mathcal{O}, \varepsilon)$ in Eq. (2), for the examined observation conditions and nominal hardware setup. Initially, no assumptions about the telescope detection efficiencies were made, i.e. transparency estimates ($\hat{T}^0_{ij}$ in Eq. (4)) were constructed for each pair of telescopes of a same type (i, j) with $d_{SP} \leq 230$ m for $\varepsilon_i = \varepsilon_j = 1$. Atmospheric transparency (T) and telescope efficiencies (ε_i) were then varied separately for the LST ($i = 1 \ldots 4$) and MST ($i = 5 \ldots 19$) sub-systems so that the sum in Eq. (5) was minimised. One telescope in each sub-system was chosen as a reference one and its efficiency, ε_R, was fixed during the optimization procedure (LST 1 and MST 5). As a result, sets of reconstructed efficiencies relative to the reference one, $\hat{\varepsilon}_i/\varepsilon_R$, were obtained for each simulated configuration (ϕ, θ, $B_\perp$). A comparison of the recovered efficiencies with the input ones ($\varepsilon_i/\varepsilon_R$) is shown in Fig. 8. By varying the reference telescope, we verified that its choice does not affect the outcome. For the LST and MST systems, the resolution of the method for the inter-calibration of the telescope responses is about 5% (2%) and 3% (3%), respectively, for the choice of configurations with $\theta = 37^\circ$ and $B_\perp/B_N = 0.3$ (0.5). The resolution is 4% (7%) and 3% (4%), respectively, for $\theta = 53^\circ$ and $B_\perp/B_N = 0.01$ (0.5).

In Fig. 9, sets of the pairwise estimates ($\hat{T}_{ij}$) corresponding to the recovered $\hat{\varepsilon}_i$ are shown for $T = 0.91$, $\theta = 53^\circ$ and $B_\perp \simeq 0$. The estimates are expressed relatively to the reference detection efficiency ε_R in terms of a quantity $q_{ij} = \hat{T}_{ij} \cdot \varepsilon_R^{-2/\gamma}$. Colored bands illustrate the spread of q_{ij} which is representative of the resolution of the atmospheric transparency estimate. Relative transparency estimates are consistent for all telescope pairs if the atmospheric conditions are uniform across the array. In the shown example, the resolution is better than 2%.

All ratios q_{ij}/q_{kl} remain constant regardless of the choice of a reference telescope but the absolute values of the estimates are not independent of it, as shown for the MSTs (red) and LSTs (blue) in Fig. 9. The ambiguity in the absolute scales of recovered efficiencies due to an arbitrary choice of a reference telescope in individual subsystems ($\varepsilon_R^{LST}, \varepsilon_R^{MST}$) has to be removed in order to achieve a coherent cross-calibration of telescopes of different types. An overall scaling factor between different telescope classes can be obtained as a ratio of sample means of q_{ij} in each subsystem, e.g. $r = \langle q^{LST} \rangle / \langle q^{MST} \rangle$. Reference efficiencies in different sub-systems can be related through the factor $r^{\gamma/2}$, e.g. $\varepsilon_R^{LST} = r^{\gamma/2} \cdot \varepsilon_R^{MST}$.

It is worth noting that the results presented in Figs. 8 and 9 were obtained for the same model of aerosol concentration, for $T = 0.91$ as used to derive the results of Section 4. Relative inter-calibration performed using the simulated data with different aerosol levels yields the optical throughput efficiencies consistent with the results presented above.

5.2. CTC as an atmospheric calibration method

We examine the CTCs calculated according to Eq. (3) for various atmospheric models. For each of the MC configurations summarized in Section 5, four different tables of the optical depth (see Section 3.3) were assumed, including the reference one used to derive the results of Section 4. The median atmospheric transparency observable by the telescopes was set to $T \in \{0.82, 0.88, 0.91, 1.00\}$, corresponding to the tropospheric, desert, navy maritime or no extinction of light due to aerosols, respectively [27]. The normalization in Eq. (2) was ascertained as $\mathcal{K} = T_R^{-1}$, where $T_R = 0.91$ is the reference value of the atmospheric model used throughout Section 4.

In order to calculate the CTCs using Eq. (3), the optical throughput of telescopes has to be obtained in advance by an independent procedure (using e.g. muon analysis [9,10] or external calibration devices [14,15]). For illustration purposes, we estimate this throughput using the relative inter-calibration described in Section 5.1, i.e. relying on the optical efficiency of the reference telescope (ε_R). It is worth noting that in reality, this approach could be used if ε_R was set by some other absolute calibration method [4]. Since no measurements were available for our study, ε_R was taken as the value ε_5 which was set as the efficiency of the reference telescope MST 5 in the MC simulations. The reference efficiency ε_R^{LST} of the LST sub-system was then set to $\varepsilon_R^{LST} = r^{\gamma/2} \cdot \varepsilon_R^{MST}$.

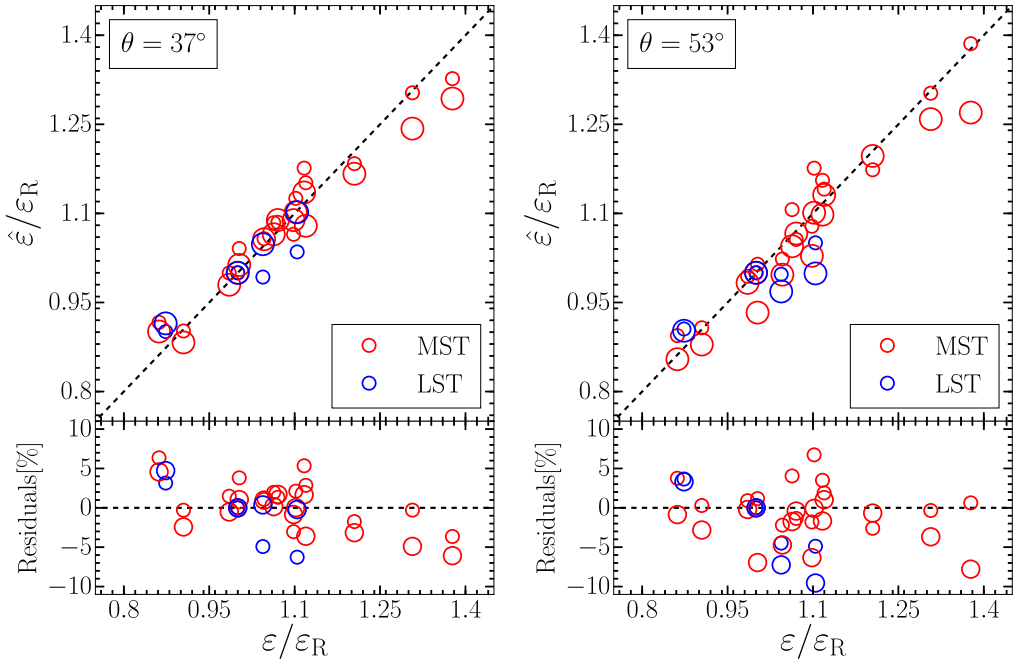

Fig. 8. Reconstructed values of the telescope optical efficiencies relative to the efficiency of the reference telescope, $\hat{\varepsilon}_i/\varepsilon_R$, are plotted against the input values chosen into simulations, $\varepsilon_i/\varepsilon_R$. The recovered efficiencies were ascertained from the inter-calibration of the simulated CTA-N array. The results are shown for $\theta = 37°$, $\phi = 3°$ (319°), $B_\perp/B_N = 0.3$ (0.5) in the left panel and $\theta = 53°$, $\phi = 355°$ (33°), $B_\perp/B_N = 0.01$ (0.5) in the right panel. Smaller markers correspond to the lower values of $B_\perp/B_N$. The percentage residuals are shown below. Dashed lines represent the equality $\hat{\varepsilon}_i/\varepsilon_R = \varepsilon_i/\varepsilon_R$.

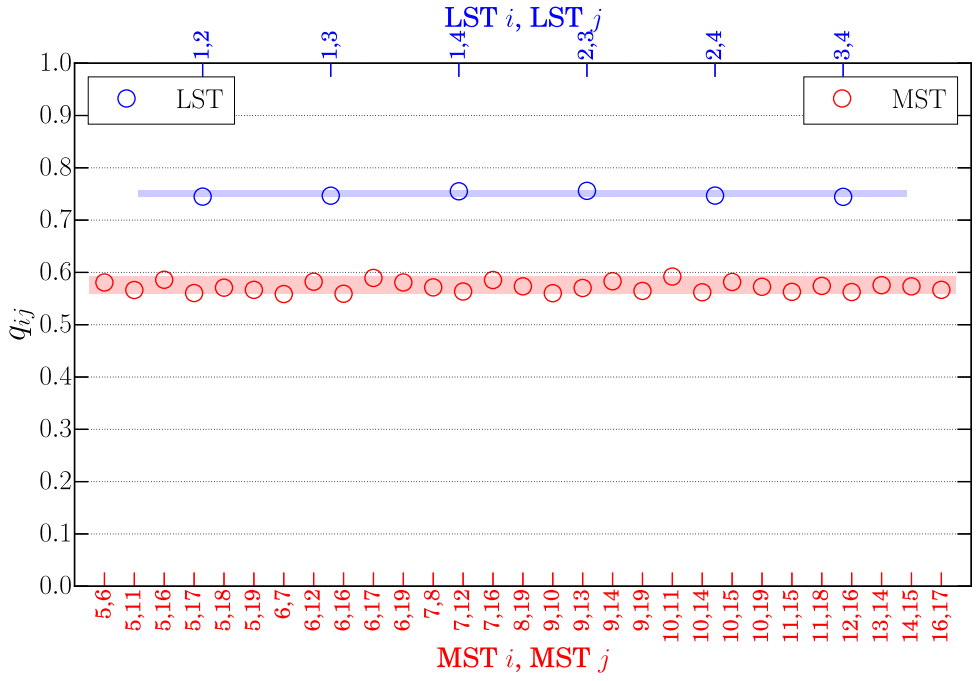

Fig. 9. Pairwise atmospheric transparency estimates relative to the optical efficiency ε_R of the reference telescope (LST 1 or MST 5), $q_{ij} = \hat{T}_{ij} \cdot \varepsilon_R^{-2/\gamma}$. These estimates are depicted for all pairs of telescopes of a same type with $d_{SP} \leq 230$ m separately for the LSTs (blue) and MSTs (red). The labels of individual telescopes are shown on the horizontal axes. Observation conditions correspond to $\theta = 53°$, $B_\perp/B_N = 0.01$ and $T = 0.91$.

In Fig. 10, the CTC estimates ($\hat{T}$) are compared with the transparency values for the atmospheric models used in MC simulations. The relative root mean square deviation of reconstructed atmospheric transparencies in the studied examples is better than 4%. Specifically, the achieved precision is better than 2% for $\theta = 37°$ and $B_\perp/B_N = 0.3, 0.5$. For $\theta = 53°$, the resolution is about 2% and 4% for $B_\perp/B_N = 0.01$ and 0.5, respectively.

An offset between the CTC estimates obtained for two different values of $B_\perp/B_N$ is present for $\theta = 53°$, as can be seen by comparing the small and big markers in the right panel in Fig. 10. We note that this effect may arise due to the influence of the geomagnetic field characterized by the values of $B_\perp/B_N$ and α (see Section 4.3). In order to verify whether this offset is systematic, a further study with increased number of MC simulations will be necessary.

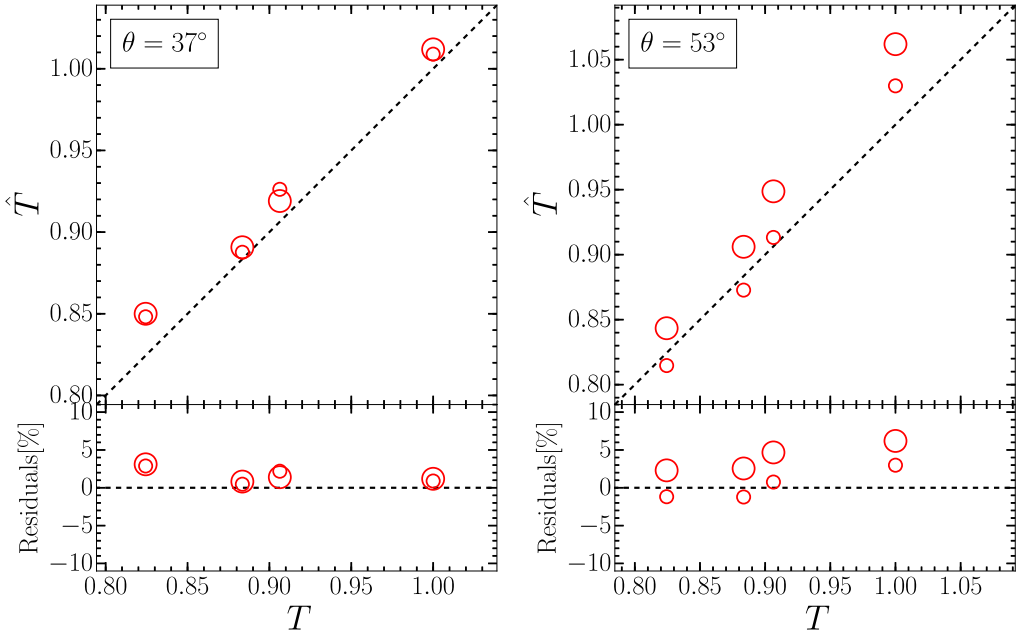

Fig. 10. The CTC estimates ($\hat{T}$) are compared to the atmospheric transparencies T inserted as input in MC simulations. Percentage residuals are shown below, dashed lines illustrate the perfect agreement. Smaller markers correspond to the lower values of $B_\perp/B_N$. For further details see caption to Fig. 8.

6. Discussion

We presented and tested a new way of calculation of the CTC [17] for its use for arrays of IACTs. The motivations for our method are the monitoring of the atmospheric transparency to Cherenkov light and the relative inter-calibration of telescope optical efficiencies. The essence of our approach is the monitoring of rates of CR-induced air showers that trigger chosen pairs of telescopes of a same type.

Atmospheric monitoring using the CTC is complementary to the calibration with the instruments anticipated for the CTA [3]. The advantages of the CTC are due to its uniqueness among the atmospheric calibration approaches that lies in the usage of telescope data taken during scientific observations (numbers of registered air showers). The CTC provides an estimate of the atmospheric transparency to Cherenkov light in the same time range and direction in which the astrophysical target is observed with excellent time resolution. Calibration using Cherenkov light estimates the atmospheric transmission in the wavelength range relevant to the function of IACTs. No dedicated equipment or calibration data acquisition are necessary for the calculation of the CTC. Hence, the application of the method does not interfere with the array's regular data taking, nor with the operation of other nearby observatories which might be of inconvenience for calibration using Lidars, for example.

Atmospheric effects influence the observations by IACTs if they take place below the altitudes of the maximum of the Cherenkov emission from air showers which happens below $\sim$12 km for showers in the CTA energy range [19]. Specifically, clouds thinner than the length of air showers (e.g. cirrus clouds) or those formed at higher altitudes have partial or no impact. Calculated using the telescope data, the CTC provides a measure of the ground layer aerosol optical depth up to the average height of CR air showers, corresponding to the energy threshold of the instrument.

The atmospheric transparency is a function of wavelength of the incident light. IACTs are sensitive to photons in a wavelength range given by the spectrum of Cherenkov light and, suitably matched, the efficiency of camera photo-sensors which peaks in the ultraviolet band (around 350 nm). Information about the wavelength dependency of the atmospheric transparency is not gathered by the telescopes and, thus, it is not provided by the CTC. Atmospheric and array calibration using the CTC will complement other dedicated devices capable of multi-wavelength calibration through usage of sources of light emitted at distinct wavelengths [14,15,33].

Array inter-calibration using the CTC is performed in a relative way, similarly to other approaches employing observational data (e.g. cosmic ray background events [34], reconstructed parameters of γ-ray-induced air showers [11,12]). The CTC algorithm can efficiently cross-check the optical throughput of all active telescopes when addressing concerns about possible discrepancies between different methods.

Regarding the accuracy of our method, it can be inferred from our estimates of the telescope trigger rates. These rates were obtained from MC simulations in various observation configurations (d, θ, β). Actual trigger rate estimates were ascertained from these simulations by extrapolation by a continuous function (see Appendix A), which was sufficient for the purpose of our feasibility study. Nevertheless, a better picture can be achieved at the expense of more extensive computations. In order to keep the trigger rate variations in individual bins below 5%, the number of bins investigated in Figs. 3 and 4 should increase at least twice for the zenith angle in the range $0^\circ - 60^\circ$ and four-times for the inter-telescope distance in the range 50–250 m.

Inaccuracies of the atmospheric transparency and the telescope optical efficiency estimates are dominated by statistical uncertainties due to computational limitations. Each data set was obtained by simulating 5×10^8 proton-initiated air showers. Out of these, $\mathcal{O}(10^3 - 10^4)$ events triggered the telescope pairs, with $\mathcal{O}(10^0 - 10^2)$ events in individual bins of energy and impact parameter. Corresponding to these numbers, the statistical uncertainties of the MC trigger rates are 10–20%. We note that during the CTA observations the statistical uncertainty of the measured trigger rate will be below 0.5% in runs of at least 10 min in duration and with a trigger rate higher than 100 Hz.

After the commissioning of the first CTA telescopes, the MC estimates of the stereo trigger rate (see Appendix A) will be verified with CTA data for various (d, θ, β) configurations, in particular for

$B_\perp/B_N \approx 0$. Estimates of the atmospheric transparency and relative optical efficiencies of telescopes obtained using the CTC concept will be cross-checked with the results of other methods and devices for atmospheric and array calibration.

As to the systematic uncertainties of the calculated estimates, they are dominated by the influence of the geomagnetic field on the air shower development. A correction of the effects of the geomagnetic field could not be found for all configurations in zenith and azimuth angles with an accuracy consistent with the CTA requirements, because of the limited computational resources. Instead, we identify the configurations of observations in which the uncertainties on the trigger rate estimates are less than a few percent, if no correction is applied.

A restriction of the systematic uncertainties can be achieved by imposing constraints on the maximum separation of a telescope pair, for example (see Section 4.3). Another option is to use only data obtained in observation runs conducted under carefully chosen zenith and azimuth angles corresponding to a smaller component of the geomagnetic field perpendicular to the air shower direction. Similar choices may result in limitations on the use of the CTC method, especially at sites with a larger magnitude of the local geomagnetic field.

A further systematic uncertainty of the CTC arises due to the precision of the optical efficiency estimates obtained using other approaches. For example, the achievable accuracy of these estimates is expected to be $\sim$4% for the muon calibration method [4].

The findings inferred from the CTC feasibility study for the LSTs and MSTs at the CTA-N location are also applicable to the CTA-S site. One of the main differences between both sites is the magnitude of the local geomagnetic field. Its total size at the Southern location is only 60% of that at the Northern site. Thus, we expect that the same constraint on (ϕ, θ), as applied to CTA-N, will result in considerably more CTA-S observation runs for which the systematic uncertainties will be below a given limit.

In addition to the differences in the local site conditions, the CTA-S array will be more complex, comprising more telescopes than CTA-N and employing a third telescope class (SSTs) [35–37]. The increased number of telescopes does not pose a problem for the application of the extended CTC concept that utilizes stereo trigger rates recorded by pairs of telescopes of the same type. Regarding the deployment of the SSTs, dedicated MC simulations (similarly to Sections 4.1 and 4.2) are foreseen in order to parameterize the SST pairwise trigger rates for different configurations (d, θ, β).

It is worth noting that a fixed configuration of the NSB was assumed in all MC simulations as the examination of different options was beyond the scope of this paper. However, the energy threshold (E_{th}) and, correspondingly, the trigger rate may change during observations with elevated levels of the NSB and stars in the telescope field of view. For example, it has been shown that the energy threshold of the MAGIC telescopes can be approximated as $E_{\mathrm{th}} \propto (NSB/NSB_{\mathrm{Dark}})^{0.4}$, where NSB is the brightness of the sky in the units of the reference brightness during dark sky conditions (NSB_{Dark}) [38].

Considering further the influence of the NSB, a procedure for the control of the individual camera pixel rates can be employed to cope with the saturation of pixels due to the higher NSB levels (e.g. bright stars). Discriminator thresholds for the individual pixel triggers are automatically adjusted according to the pixel rates, as realized for the MAGIC telescopes [39] and foreseen for the LSTs in CTA [40]. However, this induces fluctuations of the recorded telescope trigger rate close to the trigger threshold. Suitable offline cuts (e.g. application of the software trigger [41]) can further stabilize the event rate, and thus allow its use for the atmospheric monitoring. A feasibility study is planned for the implementation of the CTC under different NSB conditions and, related to that, in the LST systems with variable trigger energy thresholds.

Finally, we note that the extended CTC concept (see Section 2) can be employed also for other experiments consisting of multiple telescopes with a spacing of a few hundred meters and utilizing the imaging atmospheric Cherenkov technique in a stereoscopic regime.

7. Conclusions

A new approach to the method of the Cherenkov Transparency Coefficient has been presented as a viable option for the evaluation of the Cherenkov light extinction in the atmosphere as well as for the relative calibration of the telescope optical throughput efficiency. The outlined update of the CTC calculation is essential for applying the procedure to larger telescope arrays compared to the current generation of IACTs.

Focusing on the implementation within the future CTA observatory, the attainable accuracy of the method in explored examples has been shown to be 4% for the monitoring of the atmospheric transparency and 4–7% for the inter-calibration of telescope responses. The achieved accuracy marks an improvement with respect to the original CTC approach, compliant also with the CTA performance requirements [2].

Future studies will include the exploration of the CTC feasibility under dynamical trigger energy thresholds of the LSTs and different NSB conditions. Investigation of the trigger rate dependencies of the SSTs, for which three different designs are foreseen, is also planned for the CTC implementation at the CTA-S site.

Acknowledgments

We would like to thank Maria Concetta Maccarone and Vladimir Novotny for their insightful comments. We also thank Anthony Brown and Alison Mitchell for their careful reviews and comments that helped us to improve the paper. This work was funded by the grants LTT17006 and LM2015046 of the Ministry of Education, Youth and Sports of the Czech Republic and the grant FPA2015-69210-C6-6-R of the Spanish MINECO/FEDER, EU. This paper has undergone internal review by the CTA Consortium.

Appendix A. Fit of the geometrical dependencies of the stereo trigger rate

The dependence of the stereo trigger rate R of two telescopes of a same type on the zenith angle (in the range $\theta \in [0°, 60°]$) can be approximately described by a function

$$\hat{R}(\theta, x) = p_0 \cdot \left[p_1 \cdot \exp\left(-\frac{(\theta - p_2)^2}{p_3} \right) + \cos\theta \right], \tag{A.1}$$

where and $x = d_{\mathrm{SP}}$ is the inter-telescope distance in the shower plane (see Fig. 1). The terms in the square brackets in Eq. (A.1) account for the zenith angle dependence of the MC trigger rate normalised to $R(\theta = 0°) = 1$, see Fig. 3. The unknown parameters $p_i(x), i = 0, 1, 2, 3$, can be estimated by

$$p_0 = A \cdot [\exp(-B \cdot x) + C \cdot \exp(-D \cdot x)], \tag{A.2}$$

$$p_1 = A \cdot \exp\left(B \cdot x^C\right), \tag{A.3}$$

$$p_2 = A \cdot x + B, \tag{A.4}$$

$$p_3 = \begin{cases} A \cdot x + B, & \text{if } x \le C \\ D \cdot x + E, & \text{if } x > C. \end{cases} \tag{A.5}$$

Table A.1
Fit parameters.

	p_0	p_1	p_2	p_3
A	$(2.95 \pm 0.09) \times 10^3$	$(2.2 \pm 1.0) \times 10^{-2}$	$(5.6 \pm 0.2) \times 10^{-2}$	(1.9 ± 0.1)
B	$(2.00 \pm 0.07) \times 10^{-2}$	$(1.9 \pm 1.0) \times 10^{-1}$	33.8 ± 0.6	169.9 ± 6.4
C	$(7.7 \pm 0.3) \times 10^{-1}$	$(4.9 \pm 0.7) \times 10^{-1}$	–	264 ± 58
D	$(6.0 \pm 0.1) \times 10^{-3}$	–	–	$(6.9 \pm 0.6) \times 10^{-1}$
E	–	–	–	489.9 ± 11.3

The fit parameters A, B, C, D, E for the case of the CTA middle-sized telescopes are summarized in Table A.1. These parameters were obtained assuming that the relevant unit is degree, metre and Hertz for angles, distances and the trigger rate estimates $\hat{R}$, respectively.

References

[1] B.S. Acharya, et al., Introducing the CTA concept, Astropart. Phys. 43 (2013) 3–18, doi:10.1016/j.astropartphys.2013.01.007.

[2] M. Gaug, et al., Calibration strategies for the Cherenkov Telescope Array, in: Observatory Operations: Strategies, Processes, and Systems V, in: Proc. SPIE, 9149, 2014, p. 914919, doi:10.1117/12.2054536.

[3] J. Ebr, et al., Atmospheric calibration of the Cherenkov Telescope Array, in: Proceedings of the 35th ICRC, Busan, 2017. arXiv:1709.04273.

[4] M.C. Maccarone, D. Parsons, M. Gaug, R. de los Reyes, F. T. CTA Consortium, Tools and procedures for the CTA array calibration, in: Proceedings of the 35th ICRC, Busan, 2017. arXiv:1709.03081.

[5] G. Vasileiadis, et al., Raman LIDARs and atmospheric calibration for the Cherenkov Telescope Array, in: Proceedings of the 35th ICRC, Busan, 2017. arXiv:1709.04630.

[6] J. Ebr, P. Janecek, M. Prouza, J. Blazek, f. t. CTA Consortium, Real-time atmospheric monitoring for the Cherenkov Telescope Array using a wide-field optical telescope, in: Proceedings of the 34th ICRC, The Hague, 2015. arXiv:1508.06798.

[7] D. Mandat, et al., All sky camera for the CTA atmospheric calibration work package, in: European Physical Journal Web of Conferences, in: European Physical Journal Web of Conferences, 89, 2015, p. 03007, doi:10.1051/epjconf/20158903007.

[8] J. Juryšek, M. Prouza, Sun/Moon photometer for the Cherenkov Telescope Array - first results, in: Proceedings of the 35th ICRC, Busan, 2017. arXiv:1708.07484.

[9] M. Gaug, S. Fegan, A. Mitchell, M. Maccarone, T. Mineo, A. Okumura, Using muon rings for the optical throughput calibration of the Cherenkov Telescope Array - Part I, 2019. Submitted for publication.

[10] A.M.W. Mitchell, Optical Efficiency Calibration for Inhomogeneous IACT Arrays and a Detailed Study of the Highly Extended Pulsar Wind Nebula HESS J1825-137, Ph.D. thesis, Karl-Ruprecht University, Heidelberg, Germany, 2016. Available at http://www.archiv.ub.uni-heidelberg.de/volltextserver/21768/.

[11] W. Hofmann, Intercalibration of Cherenkov telescopes in telescope arrays, Astropart. Phys. 20 (2003) 1–3, doi:10.1016/S0927-6505(03)00137-3.

[12] A.M.W. Mitchell, R.D. Parsons, W. Hofmann, K. Bernlöhr, Cross calibration of telescope optical throughput efficiencies using reconstructed shower energies for the Cherenkov Telescope Array, Astropart. Phys. 75 (2016) 1–7, doi:10.1016/j.astropartphys.2015.10.008.

[13] R.D. Parsons, J.A. Hinton, H. Schoorlemmer, Calibration of the Cherenkov telescope array using cosmic ray electrons, Astropart. Phys. 84 (2016) 23–28, doi:10.1016/j.astropartphys.2016.08.001.

[14] A. Segreto, et al., The absolute calibration strategy of the ASTRI SST-2M telescope proposed for the Cherenkov Telescope Array and its external ground-based illumination system, in: Ground-based and Airborne Telescopes VI, in: Proc. SPIE, 9906, 2016, p. 99063S, doi:10.1117/12.2231922.

[15] A.M. Brown, On the prospects of cross-calibrating the Cherenkov Telescope Array with an airborne calibration platform, Astropart. Phys. 97 (2018) 69–79, doi:10.1016/j.astropartphys.2017.10.013.

[16] M. Gaug, On the possibility of using vertically pointing Central Laser Facilities to calibrate the Cherenkov Telescope Array, J. Instrum. 9 (2014) P07026, doi:10.1088/1748-0221/9/07/P07026.

[17] J. Hahn, et al., Impact of aerosols and adverse atmospheric conditions on the data quality for spectral analysis of the H.E.S.S. telescopes, Astropart. Phys. 54 (2014) 25–32, doi:10.1016/j.astropartphys.2013.10.003.

[18] T. Sanuki, et al., Precise measurement of Cosmic-Ray proton and helium spectra with the BESS spectrometer, ApJ 545 (2000) 1135–1142, doi:10.1086/317873.

[19] K. Bernlöhr, Impact of atmospheric parameters on the atmospheric Cherenkov technique, Astropart. Phys. 12 (2000) 255–268, doi:10.1016/S0927-6505(99)00093-6.

[20] M. Vrastil, Overview of atmospheric simulation efforts in CTA, in: Atmospheric Monitoring for High Energy Astroparticle Detectors (AtmoHEAD) 2016. Olomouc, Czech Republic, in: European Physical Journal Web of Conferences, 144, 2017, p. 01014, doi:10.1051/epjconf/201714401014.

[21] M. Gaug, CTA atmospheric calibration, in: Atmospheric Monitoring for High Energy Astroparticle Detectors (AtmoHEAD) 2016. Olomouc, Czech Republic, in: European Physical Journal Web of Conferences, 144, 2017, p. 01003, doi:10.1051/epjconf/201714401003.

[22] G. Maier, et al., Performance of the Cherenkov Telescope Array, in: Proceedings of the 35th ICRC, Busan, 2017. arXiv:1709.01381.

[23] D. Heck, J. Knapp, J.N. Capdevielle, G. Schatz, T. Thouw, CORSIKA: a Monte Carlo code to simulate extensive air showers., 1998.

[24] K. Bernlöhr, Simulation of imaging atmospheric Cherenkov telescopes with CORSIKA and sim_ telarray, Astropart. Phys. 30 (2008) 149–158, doi:10.1016/j.astropartphys.2008.07.009.

[25] M. Barcelo, et al., An analog trigger system for atmospheric Cherenkov telescopes, Ieee Trans. Nucl. Sci. 60 (2013) 2367–2375, doi:10.1109/TNS.2013.2257852.

[26] S. Sailer, et al., Trigger performance verification of the FlashCam prototype camera, Nucl. Inst. Methods Phys. Res., A (2018), doi:10.1016/j.nima.2018.08.10.

[27] A. Berk, et al., MODTRAN6: a major upgrade of the MODTRAN radiative transfer code, in: Algorithms and Technologies for Multispectral, Hyperspectral, and Ultraspectral Imagery XX, in: Proc. SPIE, 9088, 2014, doi:10.1117/12.2050433.

[28] S. Stefanik, R. de los Reyes, D. Nosek, Atmospheric monitoring and array calibration in CTA using the Cherenkov Transparency Coefficient, in: Proceedings of the 35th ICRC, Busan, 2017.

[29] C.C.G. Bowden, et al., The effect of the geomagnetic field on TeV gamma -ray detection, J. Phys. G Nucl. Phys. 18 (1992) L55–L60, doi:10.1088/0954-3899/18/2/007.

[30] G. Cocconi, Influence of the Earth's magnetic field on the extensive air showers, Phys. Rev. 95 (1954) 1705–1706, doi:10.1103/PhysRev.95.1705.4.

[31] M. Szanecki, et al., Influence of the geomagnetic field on the IACT detection technique for possible sites of CTA observatories, Astropart. Phys. 45 (2013) 1–12, doi:10.1016/j.astropartphys.2013.02.002.

[32] P. Homola, R. Engel, H. Wilczyński, Asymmetry of the angular distribution of Cherenkov photons of extensive air showers induced by the geomagnetic field, Astropart. Phys. 60 (2015) 47–53, doi:10.1016/j.astropartphys.2014.05.008.

[33] A. López-Oramas, et al., The IFAE/UAB and LUPM Raman LIDARs for Cherenkov telescope array observatory, in: Proceedings of the 33rd International Cosmic Ray Conference, Rio de Janeiro, 2013, p. 0210. arXiv:1307.5092.

[34] S. LeBohec, J. Holder, The cosmic ray background as a tool for relative calibration of atmospheric Cherenkov telescopes, Astropart. Phys. 19 (2003) 221–233, doi:10.1016/S0927-6505(02)00201-3.

[35] M.C. Maccarone, ASTRI for the Cherenkov telescope array, in: Proceedings of the 35th ICRC, Busan, 2017.

[36] I.A. Samarai, et al., Performance of a small size telescope (SST-1M) camera for gamma-ray astronomy with the Cherenkov Telescope Array, in: Proceedings of the 35th ICRC, Busan, 2017.

[37] Sol, et al., Observing the sky at extremely high energies with the Cherenkov Telescope Array: Status of the GCT project, in: Proceedings of the 35th ICRC, Busan, 2017.

[38] M.L. Ahnen, et al., Performance of the MAGIC telescopes under moonlight, Astropart. Phys. 94 (2017) 29–41, doi:10.1016/j.astropartphys.2017.08.001.

[39] J. Aleksić, et al., The major upgrade of the MAGIC telescopes, Part I: the hardware improvements and the commissioning of the system, Astropart. Phys. 72 (2016) 61–75, doi:10.1016/j.astropartphys.2015.04.004.

[40] Y. Inome, et al., Development of the camera for the large size telescopes of the Cherenkov Telescope Array, Proc. SPIE 9151 (2014), doi:10.1117/12.2054619. 9151–9151–8

[41] D. Hildebrand, et al., Higher order temperature dependence of SiPM used in FACT, in: Proceedings of the 35th ICRC, Busan, 2017.